processes

MDPI

*Article*

# Effect of Nano-$La_2O_3$ and Mo on Wear Resistance of Ni60a/SiC Coatings by Laser Cladding

**Yudong Fang [1] and Xuemei Chen [2,3,*]**

[1] Guizhou Water & Power Survey-Design Institute Co., Ltd., Guiyang 550002, China
[2] Advanced Technology Research Institute, Beijing Institute of Technology, Jinan 250011, China
[3] Intelligent Vehicle Research Institute, School of Mechanical Engineering, Beijing Institute of Technology, Beijing 100081, China
* Correspondence: chenxue781@bit.edu.cn

**Abstract:** To improve the wear resistance of the TMR blade and investigate the effect of nano-$La_2O_3$ and Mo on the wear resistance of laser cladding coating. 65Mn blade as the substrate, $La_2O_3$, Mo and Mo-$La_2O_3$ composite powders were added into Ni60a/SiC composite powder. Using scanning electron microscopy, X-ray diffraction, X-ray photoelectron spectroscopy and the CFT-I surface synthesizer, the phase composition, element distribution and friction and wear properties of the coating were analyzed to obtain the best composition of the composite coating. The results showed that the wear resistance of Mo-$La_2O_3$-Ni60a/SiC composite coating was the best. The coating was analyzed by X-ray diffraction and X-ray photoelectron spectroscopy. The coating contained hard phases such as CrB, CrC and $Cr_7C_3$, and the element distribution was uniform. It can be seen from the scanning electron microscope that the addition of nano-Mo and $La_2O_3$ improves the toughness and compactness of Ni60a/SiC composite coating, and the microstructure is refined. The friction coefficient of Mo-$La_2O_3$-Ni60a/SiC composite coating is 0.5, and the wear depth is 12.35 μm, 23% and 89% lower than that of 65Mn substrate, respectively. The surface roughness of the Mo-$La_2O_3$-Ni60a/SiC coating after wear is 2.06 μm, and the wear amount is 0.001 g. The wear mechanism of the coating is mainly adhesive wear, abrasive wear, and oxidation wear. The wear surface of the Mo-$La_2O_3$-Ni60a/SiC composite coating is mainly composed of micro furrows, accompanied by the generation of new wear-resistant layers.

**Keywords:** laser cladding; composite coating; friction and wear; microstructure

check for updates

**Citation:** Fang, Y.; Chen, X. Effect of Nano-$La_2O_3$ and Mo on Wear Resistance of Ni60a/SiC Coatings by Laser Cladding. *Processes* **2023**, *11*, 850. https://doi.org/10.3390/pr11030850

Academic Editors: Muhammad Aamir and Israr Ud Din

Received: 20 February 2023
Revised: 5 March 2023
Accepted: 9 March 2023
Published: 13 March 2023

**Copyright:** © 2023 by the authors. Licensee MDPI, Basel, Switzerland. This article is an open access article distributed under the terms and conditions of the Creative Commons Attribution (CC BY) license (https://creativecommons.org/licenses/by/4.0/).

## 1. Introduction

Wear is one of the main failure modes of agricultural machinery parts [1]. For example, a key component of a total mixing ration (TMR) forage mixer for kneading and cutting agricultural materials is the 65Mn blade. The blade surface is damaged via wear after long use, which seriously affects the working efficiency and service life of a TMR forage mixer [2–4].

Laser-cladding technology uses a high-energy-density laser beam to melt and solidify the cladding material on the substrate surface [5]. Laser absorption and other indicators have a large influence on the quality of the cladding [6,7]. Laser-cladding coated substrates significantly improve material savings, processing accuracy, surface quality and mechanical properties compared to conventional manufacturing [8]. A matrix with a laser-cladding coating provides improved mechanical properties and wears resistance. Thus, laser-cladding technology has been applied in industry and agriculture [9–11]. Following the emergence of composite materials in recent years, laser-cladding materials have gradually changed from single alloys and ceramics to composite materials [12]. In the composites, both rare earth oxides ($La_2O_3$, $CeO_2$ powder) and Mo powder can improve the microstructure and morphology of the laser cladding coating, refine the grains, and

improve the microstructure and toughness [13,14]. In the two composite coatings, Yuan et al. [15] used 45CrNi steel as the substrate and added Mo and $CeO_2$ to the Ni-based alloy by laser cladding technology, respectively, to study the microstructure and abrasive wear properties of the coating. The results showed that the coating's microstructure toughness and wear resistance were improved by adding Mo to the Ni-based alloy, and the strengthening effect of Mo on the abrasive wear properties of the coating was better than that of $CeO_2$. Wenhu Li et al. [16] prepared the composite powder of Mo-Si-B and $La_2O_3$ on the metal surface by liquid-liquid (L-L) doping, mechanical alloying (MA), and hot-pressing (HP) sintering technology to improve the wear resistance of 1173 K metal. The relationship between wear resistance and the load was analyzed. The results showed that the formation of $MoO_3$ film on the worn surface changes the contact state of the friction pair. The friction coefficient of Mo-Si-B alloy decreases and the wear rate of the alloy increases with the test load.

However, the processing technology is too complex. Houan Zhang et al. [17] combined self-propagating high-temperature synthesis (SHS) and hot pressing (HP) to prepare $La_2O_3$-WSi-$MoSi_2$ composite cladding layer on the surface of alloy steel. The wear resistance of MoSi2 against steel is significantly improved by adding both $WSi_2$ and $La_2O_3$, and it is attributed to the increase in hardness and toughness of the composite. Li et al. [18] used Mo-25Si-8.5B alloy as the basic formula to explore the effect of $La_2O_3$ content on its hardness and friction, and wear properties. The results showed that the $La_2O_3$ content affected the hardness of Mo-25Si-8.5B alloy coating. When the $La_2O_3$ content was 0.9%, the hardness and friction resistance of the composite coating was the best. Jing et al. [19] melted Ni-Mo-Si composite powder on AISI 1045 steel surface by laser cladding but only explored the oxidation resistance of the surface.

The research on the improvement of the wear resistance of the composite coating by rare earth $La_2O_3$ and Mo is extensive, but the treatment process is complex. Through the laser cladding technology, there are few studies on the influence of nano-$La_2O_3$ and Mo powder on the wear resistance of Ni60a/SiC composite powder coating. In this paper, the effects of the optimal addition of 2 wt.% nano-rare-earth $La_2O_3$ and 3.5 wt.% nano-Mo powder on the microstructure and wear resistance of Ni60a/SiC composite powder cladding layer were analyzed by laser cladding technology.

## 2. Materials and Methods

### 2.1. Materials

A steel 65Mn was cut into 60 mm × 34 mm × 5 mm specimens using an EDC wire cutting machine (ZTE CNC machine tool plant, Shenzhen, China) as a matrix for laser-cladding. The element composition of the 65Mn blade was analyzed using a direct reading spark spectrometer (FOUNDRY-MASTER PRO, Oxford, UK), as listed in Table 1. Before laser-cladding, the cladding surface was polished using #80, #120, #240, #360 and #800 sandpaper. We select Ni60A (45~106 μm; purity > 99.9%) as the basic powder of the cladding layer, SiC (70 μm, purity > 99.9%), $La_2O_3$ rare earth powder (40 nm, purity > 99.9%) and Mo powder (50 nm, purity > 99.9%) as the reinforcing phase, and the matching parameters are shown in Table 2. The ND-PM-1L ball mill (Nanjing Nanda Instrument Factory, Nanjing, China) was used to mix the powder evenly. The speed of the ball mill was 400 r/min, and the mixing time was 4 h. For ease of expression, each mixed powder and corresponding coating is labeled in Table 2.

**Table 1.** Elemental composition of 65Mn blade.

| Material | Element Composition (wt.%) | | | | | | | | |
|---|---|---|---|---|---|---|---|---|---|
| | C | Mn | Cr | Si | Ni | Cu | P | S | Fe |
| 65Mn | 0.189 | 1.034 | 0.224 | 0.272 | 0.014 | 0.1782 | 0.011 | 0.0112 | Bal |

**Table 2.** Proportioning scheme of laser cladding powder.

| Sample | Name |
|---|---|
| 65Mn | Y1 |
| 80 wt.% Ni60a + 20 wt.% SiC | Y2 |
| 78 wt.% Ni60a + 20 wt.% SiC + 2 wt.% $La_2O_3$ | Y3 |
| 76.5 wt.% Ni60a + 20 wt.% SiC + 3.5 wt.% Mo | Y4 |
| 74.5 wt.% Ni60a + 20 wt.% SiC + 2 wt.% $La_2O_3$ + 3.5 wt.% Mo | Y5 |

### *2.2. Laser-Cladding Parameters*

Laser-cladding experiments were carried out under maximum power of 5 kW of a $CO_2$ laser-cladding system (Jiangsu Zhufeng Optoelectric Technology Co., Ltd., Nantong, China). Figure 1 shows the schematic diagram of the laser cladding. The process parameters of the laser cladding are shown listed in Table 3. The cladding dimensions of the 65Mn matrix length × width = 40 mm × 20 mm, the micro-hardness of the coating was measured by a micro-hardness tester. The test load was 0.98 N, and the retention time was 10 s. The average value of five points was measured in the same area.

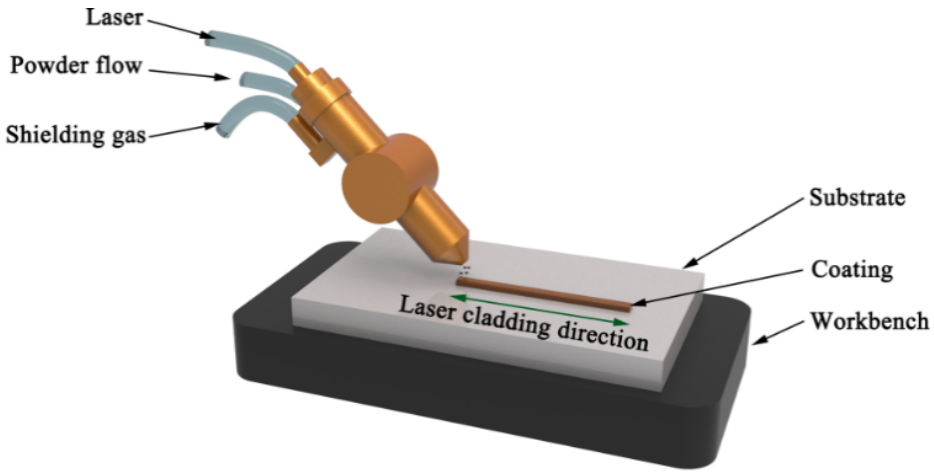


**Figure 1.** Schematic diagram of laser cladding.

**Table 3.** Parameters for laser cladding.

| Process Parameters | Operation Range |
|---|---|
| Laser power (W) | 2000 |
| Scanning speed (mm/min) | 400 |
| Spot diameter (mm) | 3 |
| Overlap rate (%) | 45 |
| Defocus distance (mm) | 10 |
| Powder feeding rate (g/min) | 8 |
| Protecting gas (Ar, L/min) | 8 |

### *2.3. Wear Test*

Friction and wear experiments were performed using a CFT-I surface comprehensive tester (China Kehua Science and Technology Development Co., Ltd., Fujian, China). Before the wear test, surface polishing of the 65Mn base cladding layer was sequentially carried out by an MP-2B metallographic sample grinder (Yantai Huayin Test Instrument Co., Ltd., Yantai, China) using #80, #120, #240, #400, #800, #1000 and #2000 round gold coherence abrasive paper. A JPS-20B ultrasonic cleaner was used to oscillate for 6 min at 40 °C. The solution was anhydrous ethanol (concentration ≧ 99.7%). In the wear test, the loading

force was 30 N, the rotating speed was 300 r/min, and the loading time was 30 min. The rotating friction mode was adopted, and the rotating radius was 3 mm. The wear amount was measured using a JM-B5003 electronic balance (Grade Ming Weighing and Checking Equipment Co., Ltd., Shenzhen, China) with an accuracy of 0.001 g. Three experiments were performed on each sample to reduce errors.

### *2.4. Microscopic Morphology Characterization*

Metallographic samples were intercepted along the direction perpendicular to the processing of the cladding samples. The samples were ground, polished and corroded ($HF:HNO_3:H_2O$ = 1:3:46). Field emission scanning electron microscopy (SEM) and three-dimensional surface topography (Nanovea ST400, NANOVEA, Irvine, CA, USA) were used to investigate the wear scar and polished sections of the coating, It enables the testing of material surfaces from nanometres to millimetres in terms of roughness, depth and other indicators, with high measurement accuracy. X-ray photoelectron spectroscopy (XPS) was used to analyze the chemical and valence compositions of the coating. The phase composition of the coating was determined by X-ray diffraction (XRD). The scanning speed was 3°/min, and the scanning angle was 10° to 90°.

## 3. Results and Discussion

### *3.1. Micro-Hardness and Phase Analysis of the Coatings*

Figure 2a shows the micro-hardness of the sample, and the hardness of 65Mn substrate is 608 HV. the hardness of the cladding layer on 65Mn substrate is improved by laser cladding technology. The surface hardness of Y2, Y3, Y4 and Y5 are 870 HV, 991 HV, 914 HV and 1285 HV, respectively. The hardness of the cladding layer is higher than that of the Ni60a/SiC cladding layer after adding nano-$La_2O_3$ and Mo, which indicates that nano-$La_2O_3$ and Mo refine the grains of the Ni60a/SiC composite cladding layer. The refinement of the grains is beneficial to the improvement of the hardness of the cladding layer, and the ability of nano-$La_2O_3$ to inhibit grain growth is better than that of Mo powder. The hardness of the Ni60a/SiC composite coating reached 1285 HV when the nano-$La_2O_3$ and Mo powder were mixed, which indicates that the growth of the crystal is further inhibited, and the hardness is significantly improved.

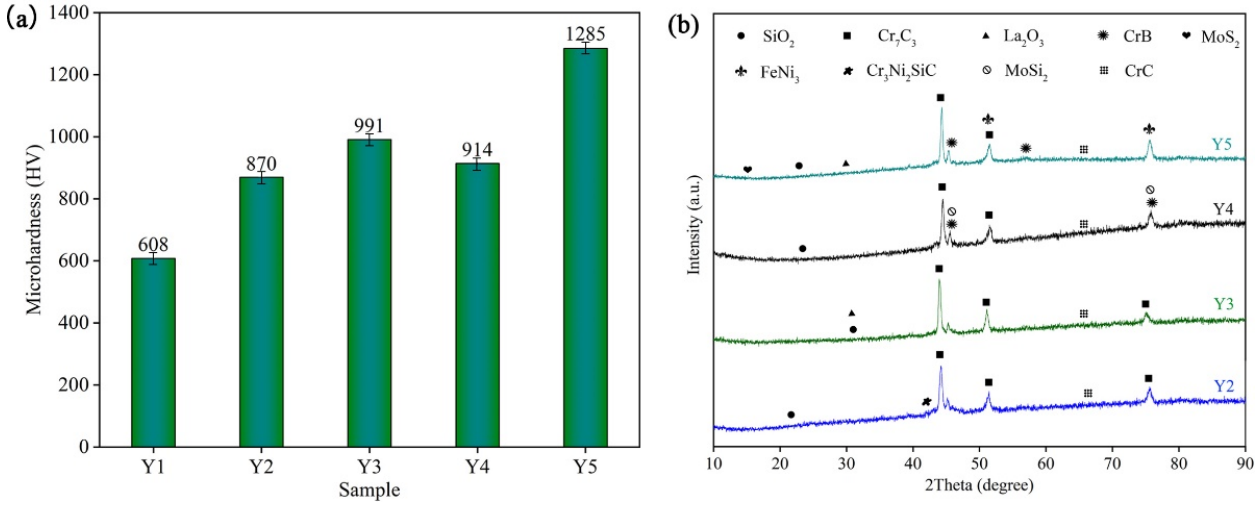


**Figure 2.** Micro-hardness (**a**) and XRD pattern (**b**) of the composite coating.

Figure 2b shows that the formation of Y2, Y3, Y4 and Y5 coatings is accompanied by a variety of new phases, indicating that the composite powder is decomposed and ablated at high temperatures of laser cladding. $CeO_2$, CrB, CrC and FeNi3 are formed in the coating as primary phases, and $CeO_2$ and CrC have no obvious diffraction peaks. Y3 and Y5 are added with nano-$La_2O_3$, and the rare earth lanthanum is stable in the oxide coating.

Mo powder, Si, S, and other elements formed MoSi2 and MoS compounds in the coating added with nano-Mo powder. The addition of nano-$La_2O_3$ and Mo powder improved the microstructure of the coating and are beneficial to the refinement of other grains. At high temperatures, the coating recrystallization occurred, and the elements were combined with various intermetallic phases [20]. $Cr_7C_3$ and Cr3Ni2SiC are the hard phases of secondary precipitation in the coating. Under the same laser cladding parameters, the diffraction peak intensity of $Cr_7C_3$ in the Y5 coating is the largest, related to the precipitation of $Cr_7C_3$ in the coating. Combined with the CrC phase in the primary phase, the formation of the hard phase of the coating is conducive to improving the hardness of the composite [21]. The affinity between C and Cr is strong, and CrC and $Cr_7C_3$ phases result from an in-situ reaction between Cr and graphite in the molten pool [22]. Studies have shown that carbides precipitated at grain boundaries can improve the wear resistance of materials [23].

### *3.2. Wear Test Analysis*

Figure 3 is the data diagram of the friction coefficient and wear amount of coating samples, and Figure 3c is the wear schematic diagram. From Figure 3a,b, it can be seen that the friction coefficient of Y1 jumps greatly within 30 min and does not tend to a stable value. The friction coefficient changes between 0.5 and 0.8, and the average friction coefficient is about 0.65. After 15 min running-in stage, the friction coefficient gradually tends to be stable at around 0.5. The running-in stage shows that the wear layer has been destroyed and tends to be stable after 15 min. The friction coefficient of Y2 is 23% lower than that of Y1.

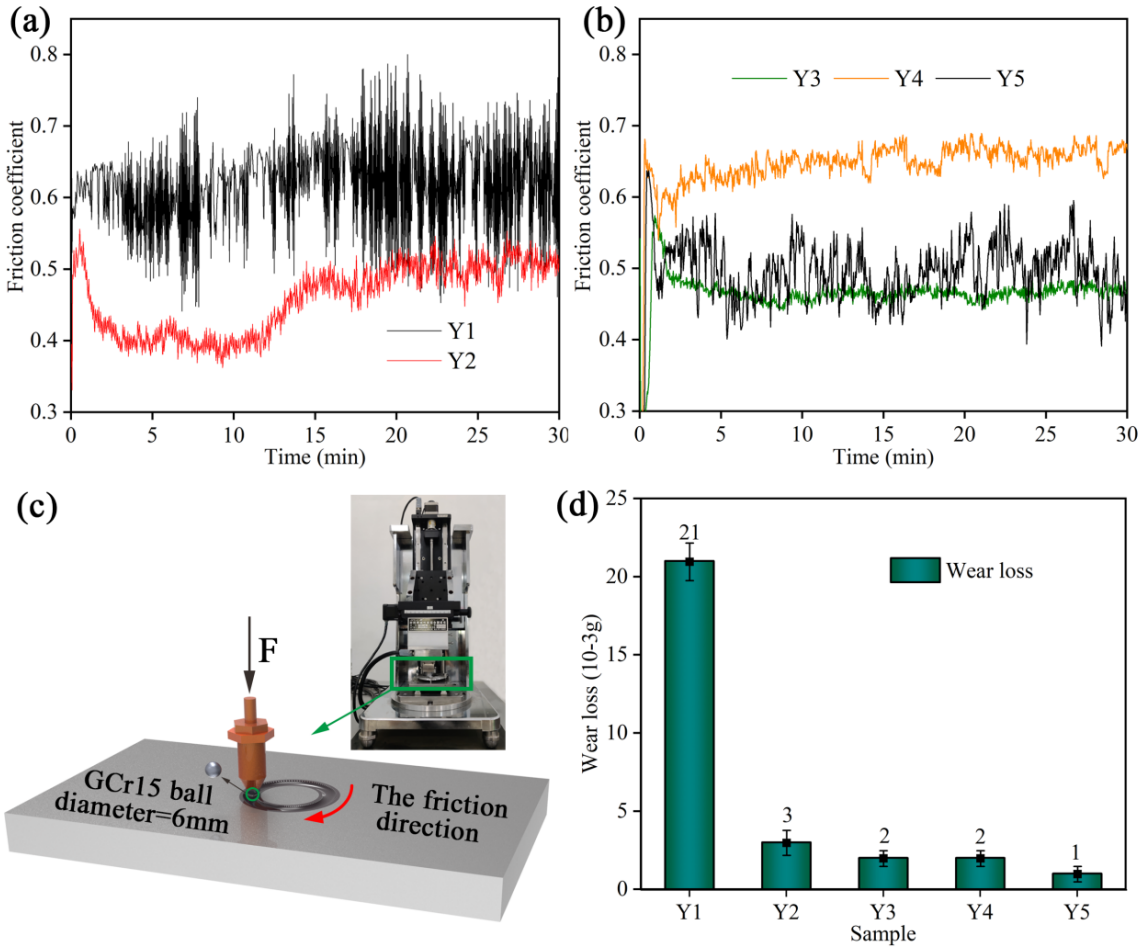


**Figure 3.** The curve of friction coefficient for (**a**) M1 and M2, (**b**) M3, M4, M5 and M6. (**c**) Wear schematic. (**d**) Wear loss analysis.

It can be seen from Figure 3b that the friction coefficients of Y3 and Y5 are stable around 0.46 and 0.63 within 30 min, respectively, and there is no long wear running-in stage, indicating that the wear failure of the wear layer is relatively light. The friction coefficients of Y3 and Y5 are reduced by 29% and 3% compared with Y1, respectively. The friction coefficient of Y5 has a noticeable jump within 30 min, which indicates that the wear layer of Y5 was varied during wear failure, and the average friction coefficient is about 0.5. The friction coefficient of Y5 is reduced by 23% compared with Y1. Figure 3d shows the wear analysis of the sample. The average wear amount of Y1 is 0.021 g, and the wear amounts of Y2, Y3, Y4 and Y5 are 0.003 g, 0.002 g, 0.002 g and 0.001 g, respectively. It can be seen that the wear amount after laser cladding is significantly reduced. Combined with Figure 2, it can be seen that the reduction of wear amount is related to the generation of the hard phase of the coating, and the wear amount of Y5 is the least.

### *3.3. Microscopic Wear Morphology Analysis*

Figure 4a,e shows the three-dimensional morphology and SEM images of the wear scar of the coating sample. Combined with the data in Figure 4f, it can be seen that the surface roughness of the Y1 coating sample after wear is 23.43 μm, and the average wear depth is 110.06 μm. It can be seen from the observation of the wear scar (Figure 4a) that there are serious cracks and deep grooves on the worn surface, a serious drawing phenomenon and no new wear-resistant layer. The analysis of laser cladding coating shows that the wear scar depth and surface roughness under the coating is significantly reduced. The surface roughness of Y2, Y3, Y4 and Y5 are 3.93 μm, 2.20 μm, 3.41 μm and 2.06 μm, respectively. The surface roughness of Y3 and Y5 is the lowest. The average wear depths of Y2, Y3, Y4 and Y5 are 19.21 μm, 15.34 μm, 15.79 μm and 12.35 μm, respectively. The average wear depth of Y5 is the smallest, and the wear depth of Y5 is reduced by 89% compared with Y1.

Figure 4b,e shows that the wear surface of the coating is significantly improved compared with that of 65Mn substrate. The wear surface of Y2 appears delamination, and with the emergence of a new wear-resistant layer, the wear surface of Y3 appears to have abrasive grains and grooves. Combined with Figure 3b, the generation of abrasive particles reduced wear to a certain extent, so the friction coefficient decreased. The wear surface of Y4 appeared to be coating cracking, and the coating peeled obviously. The instability of the wear-resistant layer caused an increase in the friction coefficient. The wear surface of Y5 appeared to have abrasive particles and furrows, but the wear of the coating was lighter and accompanied by the emergence of new wear layers. Combined with Figure 3b,d, the low friction coefficient of Y5 is related to the surface roughness of the worn surface and the formation of a new wear-resistant layer, which leads to a decrease in wear depth.

Figure 4 shows that the wear width of Y1 is the largest and Y5 is the smallest. Serious fatigue and mechanical wear occur on the wear surface of Y1, and the wear resistance is poor. In contrast, the wear surface of the sample containing the coating is significantly improved. Combined with Figure 2, the formation of the coating hard phase is one of the reasons for the improvement of wear resistance. The Y2 wear surface is mainly adhesive, and Y3 has significant abrasive wear. There are abrasive particles on the wear surface, generally generated under cyclic stress, and most of the abrasive particles are oxides. In the friction heat environment, $CeO_2$ abrasive particles can be retained on the interface as a lubricant, forming a wear-reducing layer under cyclic stress, reducing the further wear of the surface and reducing the friction coefficient [24]. The delamination phenomenon caused by fatigue wear occurs in Y4, and the wear surface of Y5 is dominated by micro-furrows. Based on the above analysis, $La_2O_3$ improves the wear resistance of Ni60a/SiC coating better than Mo powder, and Y5 shows the best comprehensive performance and wear resistance.

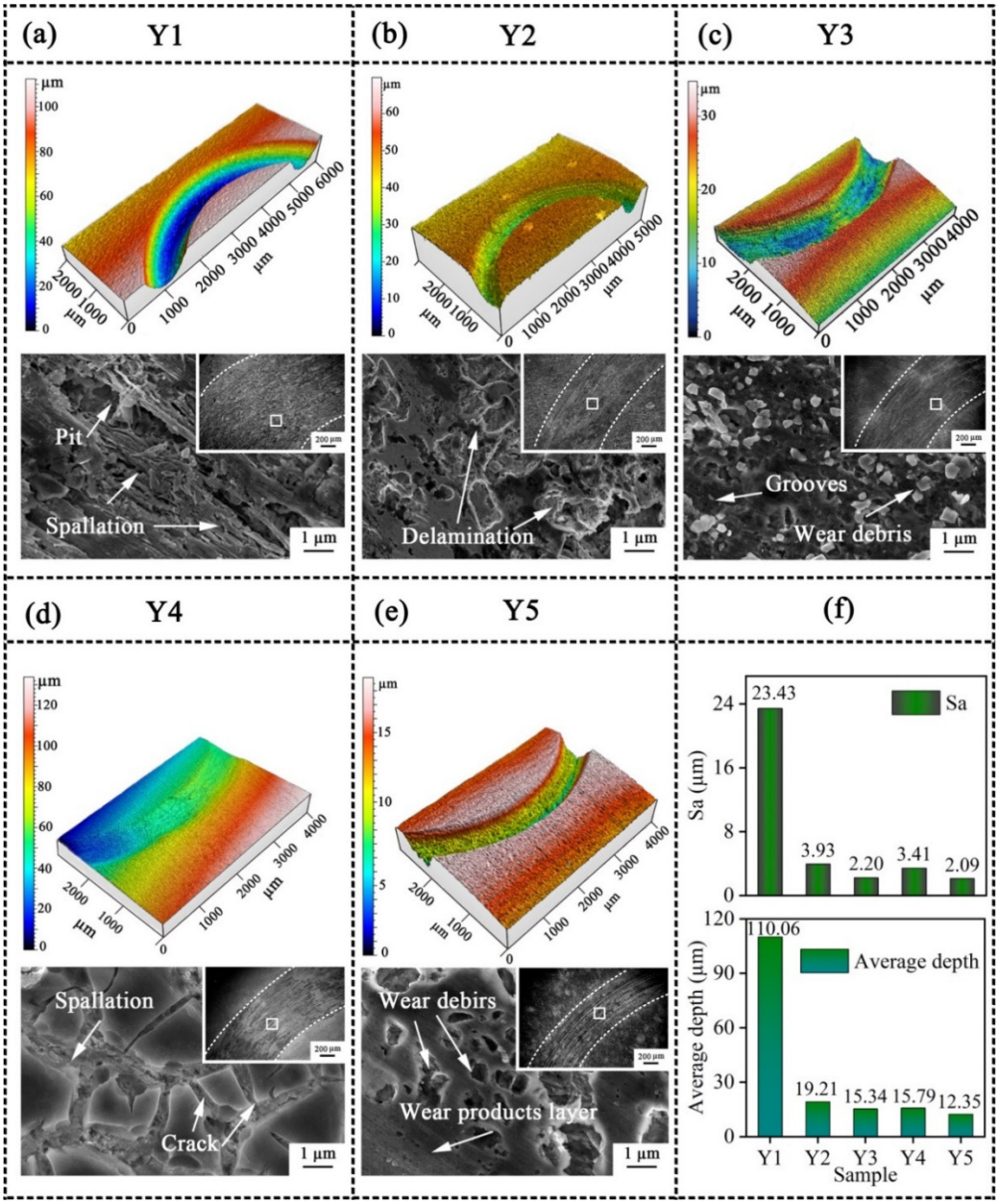


**Figure 4.** Three-dimensional morphology and SEM image of coating: (**a**) Y1, (**b**) Y2, (**c**) Y3, (**d**) Y4, (**e**) Y5. (**f**) Surface roughness (Sa) of wear specimens and average wear depth.

### *3.4. Elemental Analysis of Coating*

Figure 5a shows that the content of C and Mn in the wear scar of the 65Mn matrix is 58.43% and 22.38%, and hard phase elements Si, Cr and Ni are 2.08%, 0.04% and 13.52%, respectively. In the coating sample, the content of hard phase elements is significantly increased. The contents of Si in the wear scars of Y2, Y3, Y4 and Y5 are 7.59%, 7.23%, 9.70% and 5.39%, respectively. The contents of Cr are 15.92%, 19.65%, 14.44% and 15.83%, respectively. Combined with Figures 2–4, hard phase elements could reduce the friction coefficient and wear amount of the wear surface, improve the wear state of the wear surface, and improve the wear resistance of the coating. Compared with the element content in the wear scar and unweared parts of the coating (Figure 5d,f,h), the Si content in the unweared parts of Y3, Y4 and Y5 is 7.28%, 7.38% and 7.20%, respectively, and the Cr content is 21.12%, 29.77% and 28.54%, respectively. The element content was higher than the wear area, indicating that the coating element was slightly shifted when the wear occurred. Compared

with the change in the coating's oxygen (O) content, the content of unweared Y3, Y4 and Y5 is 6.46%, 1.69% and 2.66%, respectively. And oxygen content is 11.69%, 22.50% and 23.11%, respectively. The oxygen content increased obviously, indicating the oxidation reaction occurred in the wear layer, in which $CeO_2$ as oxide abrasive particles had the effect of lubricant. Combined with Figures 3 and 4, the friction coefficient of the Y5 surface is small, and the change of wear surface was small.

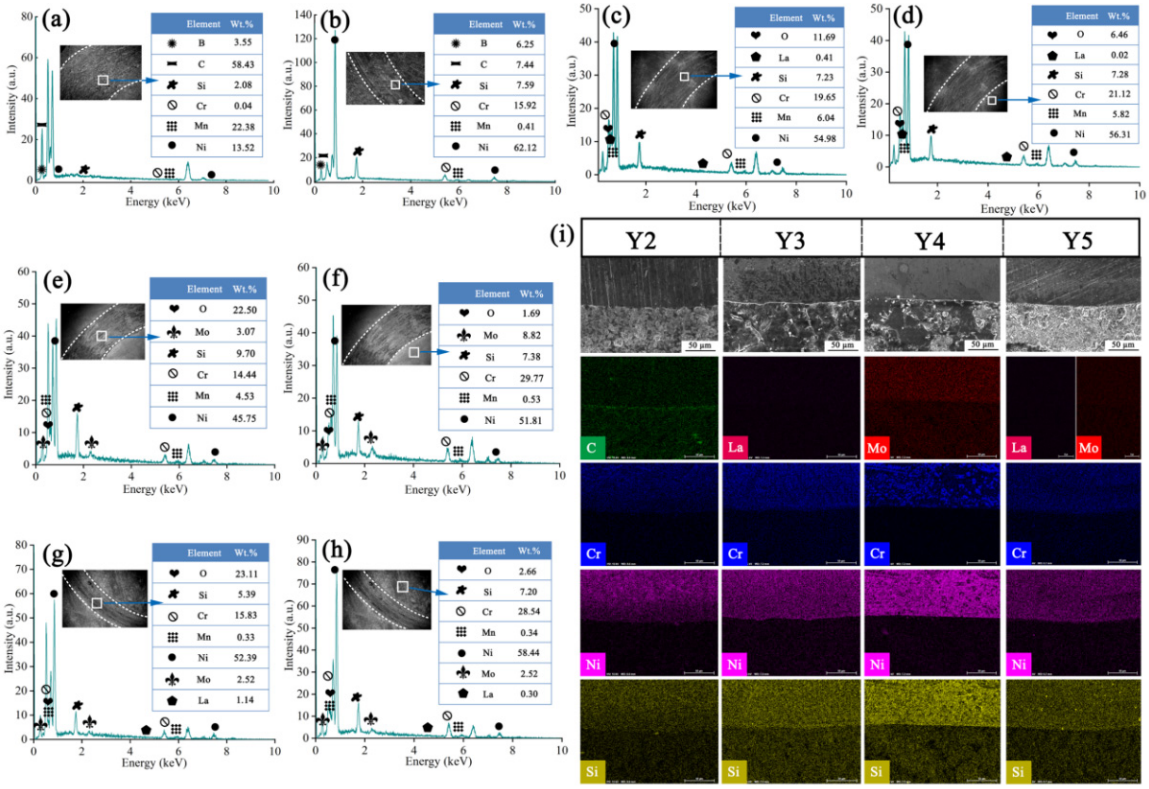


**Figure 5.** Element Analysis of Wear Surface of Sample: (**a**) Y1, (**b**) Y2, (**c**,**d**) Y3, (**e**,**f**) Y4, (**g**,**h**) Y5. (**i**) EDS mapping of Y1~Y5.

To analyze the influence of nano-rare earth $La_2O_3$ and Mo on the Ni60a/SiC composite powder cladding layer, the element distribution in the cross-section of Y2, Y3, Y4 and Y5 coatings is observed (Figure 5i). It can be seen from the figure that the coating is rich in Cr, Ni and Si, which is the main element of the cladding powder. Compared with the Y2 composite powder coating, the composite coating with nano-rare-earth $La_2O_3$ and Mo is dense without obvious cracks and holes, indicating that nano-rare-earth $La_2O_3$ and Mo can promote the uniform refinement of microstructure and promote the uniform distribution of Cr, Ni and Si elements in the coating, indicating that nano-rare-earth $La_2O_3$ and Mo can improve the fluidity of Cr, Ni and Si elements in the coating. The ionic radius of $La^{3+}$ is large, which can effectively hinder the transfer of substances [13]. The distribution of Si and Ni in Y2 coating with nano-Mo is uniform, and the Cr element is partially vacant. Compared with Y2 coating, the distribution of elements in Y3 and Y5 coating with rare earth $La_2O_3$ is more uniform, and the mutual infiltration of Cr and Si elements with the substrate promotes the better combination of the coating and the substrate, which is beneficial to improve the comprehensive performance of the coating.

To further understand the effect of nano-$La_2O_3$ and Mo powder on the Ni60a/SiC composite cladding layer and analyze the composition and chemical state of the coating, XPS analysis was carried out on Y3, Y4 and Y5. From Figure 6, it can be seen that the coating contains basic hard phase elements such as Cr, Ni and Si. On the $Cr_{2p}$ orbital, the binding energies of Cr elements are in the range of 570~590 eV. The valence states of Cr elements in the three coatings are composed of multiple binding energies, and the

difference is small. Y3, Y4 and Y5 contain $Cr_2O_3$, and the binding energy is about 575.6 eV. $Cr_2O_3$ is easy to form, which is related to the high affinity between O and Cr and the low Gibbs free energy of $Cr_2O_3$ [25,26]. Compared with the change of the binding energy of nano-$La_2O_3$ and Mo compounds in the coating, the 3d orbitals of La in Y3 and Y5 have multiple linear spectral splittings (Figure 6a,c). This is because La mostly exists in the form of compounds. Combined with the binding energy diagram of O1s, the binding energy of La and O1s is low, about 528.6 eV, and the La$3d_{5/2}$ orbit does not show obvious diffraction peaks. The binding energy of the La$3d_{5/2}$ orbit in Y3 is 837.9 eV, and that of the La$3d_{5/2}$ orbit in Y5 is 836.7 eV. There is a significant deviation in the binding energy.

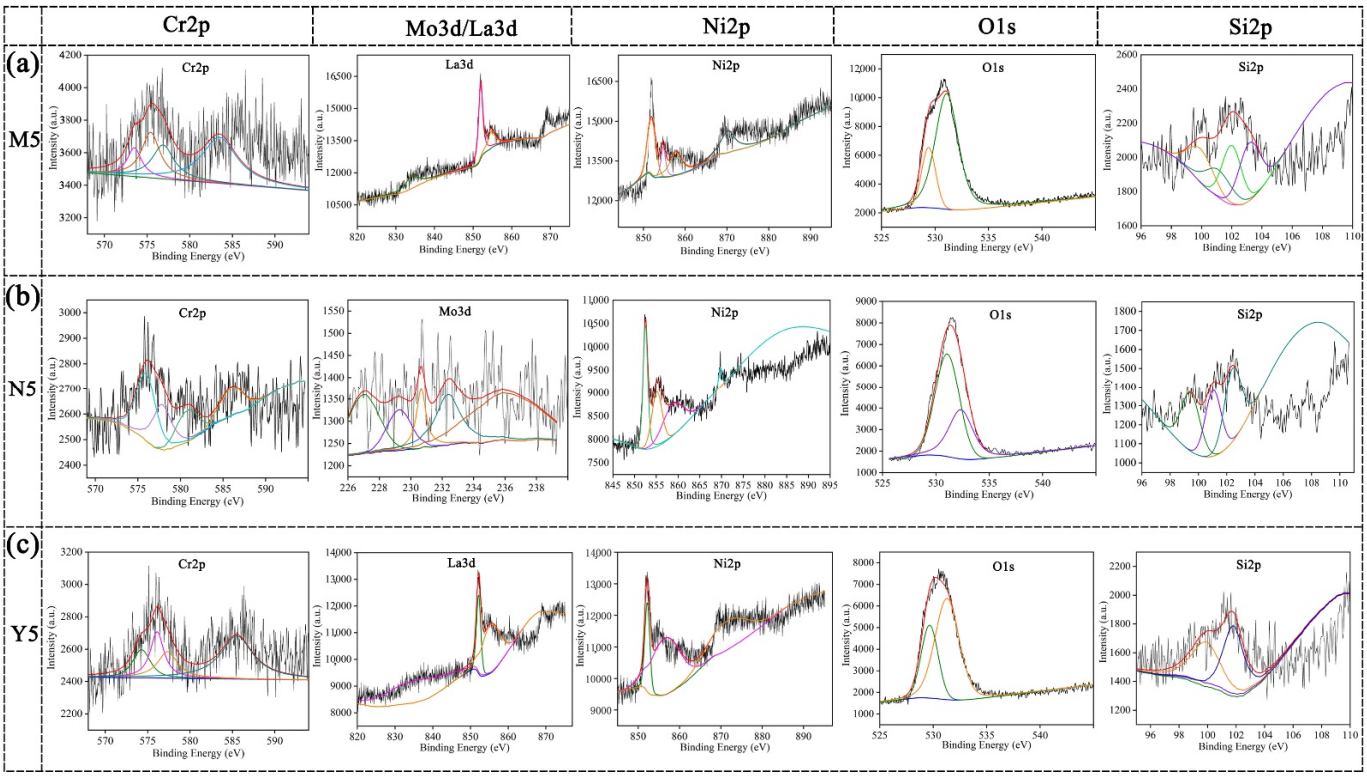


**Figure 6.** XPS Analysis of Y3, Y4 and Y5 Coating.

The binding energy of La$3d_{3/2}$ orbits of Y3 and Y5 is around 852.0 eV. After multiple line spectrum splitting, the difference in the binding energy of La$3d_{3/2}$ orbits in Y3 is 2.7 eV, and that of La$3d_{3/2}$ orbits in Y5 is 3.2 eV. The diffraction peak of Mo in Figure 6b is observed, and the photoelectron peak of Mo is very weak. On the other hand, the diffraction peak of the Mo3d3/2 orbit is relatively high, and the binding energy is 231.1 eV.

In the Ni2p orbit, Y3, Y4 and Y5 have obvious spin-orbital splitting and have satellite peaks. The binding energy of Ni$2p_{3/2}$ orbit in Y3 is 851.8 eV and 854.6 eV. The binding energy of Ni$2p_{3/2}$ orbit in Y4 is 852.4 eV and 855.4 eV. The binding energy of Ni$2p_{3/2}$ orbit in Y3 is 852.1 eV and 854.6 eV. The binding energy of Ni$2p_{1/2}$ orbit in Y3, Y4 and Y5 are 870.5 eV, 869.7 eV and 868.3 eV. The binding energy difference between the Ni$2p_{3/2}$ orbit and Ni$2p_{1/2}$ orbit is 18.7 eV, 17.3 eV and 16.2 eV. It can be seen from the binding energy that Ni exists in the oxide film in the chemical state of $Ni^{2+}$. On the 2p orbit of Si, the binding energies of Y3 at 103.2 eV, 101.9 eV and 99.6 eV correspond to the orbits of $CeO_2$, Si3N4 and Si2p3/2, respectively. The binding energies of Y4 at 102.5 eV, 101.0 eV and 99.4 eV correspond to the orbits of $CeO_2$, SiC and Si$2p_{3/2}$, respectively. The binding energies of Y5 at 101.9 eV and 99.7 eV correspond to the orbits of $CeO_2$ and Si$2p_{3/2}$, respectively. Compared with Y3, Y4 and Y5, Si3N4 and SiC were not found in Y5, indicating that $Si_3N_4$ and SiC gradually replaced $CeO_2$, which promoted the anti-wear performance of Y5 coating. Combined with Figure 2, Y3, Y4 and Y5 coatings had hard phase and anti-wear elements.

Compared with Y3 and Y4, the anti-wear $CeO_2$ content of Y5 coating increased, and the improvement of wear resistance of Y5 coating was closely related to the decrease of friction coefficient and $CeO_2$ content.

## 4. Conclusions

(1) Ni60a/SiC, Mo-Ni60a/SiC, $La_2O_3$-Ni60a/SiC and Mo-$La_2O_3$-Ni60a/SiC coatings produced hard phases such as CrC and $Cr_7C_3$ and lubrication $CeO_2$ phases under the same laser cladding process. Compared with Ni60a/SiC coating, the coating with nano-$La_2O_3$ and Mo powder is accompanied by the generation of new phases such as FeNi3, MoSi2 and Cr3Ni2SiC, which significantly improved the structure of the coating and improved the hardness and wear resistance of the coating.

(2) Compared with the 65Mn substrate, the coating samples show better wear resistance, and the Mo-$La_2O_3$-Ni60a/SiC coating had the best wear resistance. In the same test conditions, the friction coefficient is 0.5, and the wear depth is 12.35 μm, 23% and 89% lower than the substrate, respectively. The surface roughness of the Mo-$La_2O_3$-Ni60a/SiC coating after wear is 2.06 μm, and the wear amount is 0.001 g, a slight wear failure occurred on the coating surface.

(3) The wear mechanism of 65Mn substrate is fatigue wear and mechanical wear. The wear surface with the coating is mainly adhesive wear, abrasive wear, and oxidation wear. Adding nano-Mo powder and rare earth $La_2O_3$ improves the compactness of the coating. Mo powder enhances the toughness of the coating microstructure. Rare earth $La_2O_3$ inhibits the growth of grains and refines the microstructure. Mo-$La_2O_3$-Ni60a/SiC coating shows the best wear resistance, and the wear surface is dominated by micro furrows.

**Author Contributions:** Conceptualization, Y.F. and X.C.; methodology, X.C.; software, Y.F.; validation, Y.F.; formal analysis, Y.F.; investigation, X.C.; resources, Y.F.; data curation, Y.F.; writing—original draft preparation, Y.F.; writing—review and editing, Y.F.; visualization, Y.F.; supervision, Y.F.; project administration, X.C.; funding acquisition, X.C. All authors have read and agreed to the published version of the manuscript.

**Funding:** This research was supported by Shandong Key R & D Program (No. 2020CXGC010118) and Jinan Science and Technology Plan Project (No. 202126006).

**Data Availability Statement:** Not applicable.

**Conflicts of Interest:** The authors declare that they have no known competing financial interests or personal relationships that could have appeared to influence the work reported in this paper.

## References

1. Ning, C.T. Research on failure form, design criteria, design procedure and standardization of mechanical parts, Guide. *Sci.-Technol. Mag.* **2013**, *32*, 124.
2. Wang, T.; Wen, B.Q.; Kan, Z.; Lin, J.B. Wear behavior of different materials applied on horizontal mixer blades used in the processing of total mixed rations. *Trans. ASABE* **2019**, *62*, 1743–1753. [CrossRef]
3. Wang, T.; Kan, Z.; Li, J.B.; He, Q.; Wen, B.Q.; Li, J.J. Study on rural eco-tourism regionalization based on fuzzy evaluation-three dimensional magic cube. *J. Chin. Agric. Mech.* **2019**, *4*, 89–93+228.
4. He, Q.; Li, A.L.; Qu, W.H.; Zhang, Y.; Kong, L. Investigation on friction and wear properties of high-temperature bearing steel 9Cr18Mo. *Mater. Res.-Lbero-Am. J.* **2018**, *21*, e20170715. [CrossRef]
5. Lou, B.Y.; Chen, Z.; Bai, W.J.; Dong, G. Structure and erosion resistance of Ni60A/SiC coatting by laser cladding. *Trans. Nonferr. Met. Soc.* **2006**, *16*, 643–646. [CrossRef]
6. Shahri, P.K.; HomChaudhuri, B.; Pulugurtha, S.S.; Mesbah, A.; Ghasemi, A.H. Traffic Congestion Control Using Distributed Extremum Seeking and Filtered Feedback Linearization Control Approaches. *IEEE Contr. Syst. Lett.* **2022**, *7*, 1003–1008. [CrossRef]
7. Khorasani, M.; Ghasemi, A.H.; Leary, M.; Sharabian, E.; Cordova, L.; Gibson, L.; Downing, D.; Bateman, S.; Brandt, S.; Rolfe, B. The effect of absorption ratio on meltpool features in laser-based powder bed fusion of IN718. *Opt. Laser Technol.* **2022**, *153*, 108263. [CrossRef]
8. Khorasani, M.; Gibson, I.; Ghasemi, A.H.; Hadavi, E.; Rolfe, B. Laser subtractive and laser powder bed fusion of metals: Review of process and production features. *Rapid Prototyp. J.* **2023**, 1355–2546, *ahead of print*. [CrossRef]
9. Zhang, W.P.; Liu, S. Microstructure of Fe-Ti-B composite coating prepared by laser cladding. *Chin. J. Nonferr. Met.* **2005**, *15*, 558–564.

10. Guo, J.K. Multiphase material-an attractive trend for material research. *Res. Dev. World Sci. Technol.* **2000**, *22*, 17–18.
11. Straumal, B.B.; Klinger, L.; Kuzmin, A.; Gabriel, A.; Anna, K.; Alexander, B. High entropy alloys coatings deposited by laser cladding: A review of grain boundary wetting phenomena. *Coatings* **2022**, *12*, 334. [CrossRef]
12. Feng, X.D.; Yuan, Q.L.; Cao, J.J.; Su, Z.J. Microstructure and properties comparison of laser cladding layer and spraying layer of Ni-Based self-fluxing alloy. *Mater. Mach. Eng.* **2010**, *34*, 73–79.
13. Dong, S.Z.; Ma, Z.; Pan, R.; Li, Z.C. Application of rare earth oxides to ceramic coatings. *Electr. Finish* **2012**, *31*, 76–80.
14. Wang, Q.B.; Dou, X.W.; Chao, M.J.; Yuan, B.; Liang, E.J. Effect of Mo-doping on the microstructure and wear properties of laser-clad nickel-based coatings. *Appl. Laser* **2005**, *25*, 97–100.
15. Yuan, J.P.; Zhang, P.; Liang, Z.J.; Ma, L. Effect of Mo and $CeO_2$ on microstructure and properties of laser cladding Nickel-base alloy coatings. *Rare Met. Mater. Eng.* **2008**, *37*, 147–151.
16. Li, W.H.; Ai, T.T.; Dong, H.F.; Zhang, G.J. Tribological properties of Mo-Si-B alloys doped with La2O3 and tested at 293–1173 K. *Materials* **2009**, *12*, 2011. [CrossRef] [PubMed]
17. Zhang, H.A.; Hu, X.P.; Yan, J.H.; Chen, P.; Tang, S.W. Dry sliding wear behaviors of $La_2O_3$–$WSi_2$–$MoSi_2$ composite against alloy steel. *Wear* **2006**, *260*, 903–908. [CrossRef]
18. Li, W.H.; Fu, S.H.; Ai, T.T.; Zhou, P.D.; Chen, J.; Zhang, G.J. Effect of $La_2O_3$ on friction and wear characteristics of Mo-25Si-8.5B alloy. *Heat Treat. Met.* **2019**, *44*, 18–21.
19. Liu, J.; Chen, Y.; Zhang, J. Oxidation behavior of Ni–Mo–Si alloy coatings fabricated on carbon steel by laser cladding. *Surf. Coat. Technol.* **2019**, *375*, 903–910. [CrossRef]
20. Huebner, J.; Kata, D.; Kusinski, J.; Rutkowski, P.; Lis, J. Microstructure of laser cladded carbide reinforced inconel 625 alloy for turbine blade application. *Ceram. Int.* **2017**, *43*, 8677–8684. [CrossRef]
21. Corrêa, E.O.; Alcântara, N.G.; Valeriano, L.C.; Barbedo, N.D.; Chaves, R.R. The effect of microstructure on abrasive wear of a Fe–Cr–C–Nb hardfacing alloy deposited by the open arc welding process. *Surf. Coat. Technol.* **2015**, *276*, 479–484. [CrossRef]
22. Torgerson, T.; Mantri, S.; Banerjee, R.; Scharf, T. Room and elevated temperature sliding wear behavior and mechanisms of additively manufactured novel precipitation strengthened metallic composites. *Wear* **2019**, *426*, 942–951. [CrossRef]
23. Fayazfar, H.; Salarian, M.; Rogalsky, A.; Sarker, D.; Russo, P.; Paserin, V.; Toyserkani, E. A critical review of powder-based additive manufacturing of ferrous alloys: Process parameters, microstructure and mechanical properties. *Mater. Des.* **2018**, *144*, 98–128. [CrossRef]
24. Alidokht, S.A.; Manimunda, P.; Yue, S.; Chromik, R. Cold spray deposition of a Ni-WC composite coating and its dry sliding wear behavior. *Surf. Coat. Technol.* **2016**, *308*, 424–434. [CrossRef]
25. Róg, G.; Kozlowska-Rog, A.; Dudek, M. The standard Gibbs free energy of formation of calcium chromium (III) oxide in the temperature range (1073 to 1273) K. *J. Chem. Therm.* **2007**, *39*, 275–278. [CrossRef]
26. Sun, S.T.; Fu, H.G.; Ping, X.L.; Guo, X.Y.; Jian, L.; Lei, Y.P.; Wu, W.B.; Zhou, J.X. Effect of liquid nitrogen cooling on grain growth and properties of laser cladding in-situ (Ti, Nb)C/Ni composite coatings. *Mater. Charact.* **2019**, *152*, 115–129. [CrossRef]


**Disclaimer/Publisher's Note:** The statements, opinions and data contained in all publications are solely those of the individual author(s) and contributor(s) and not of MDPI and/or the editor(s). MDPI and/or the editor(s) disclaim responsibility for any injury to people or property resulting from any ideas, methods, instructions or products referred to in the content.